

Ali Osman Berk Şapçı

May 6, 2022

Contents

| | | |
|----------|---|-----------|
| 1 | Introduction | 1 |
| 1.1 | Challenges | 1 |
| 1.2 | Contributions | 1 |
| 2 | Biological Experiments and Data Collection | 2 |
| 3 | Feature Extraction | 3 |
| 3.1 | Construction of Pose Values and Preprocessing | 4 |
| 3.1.1 | Dealing with Occluded Body Parts | 4 |
| 3.1.2 | Aligning Flies with Different Orientations | 5 |
| 3.1.3 | Preprocessing: Filtering and Imputation | 5 |
| 3.2 | Computation of Spatio-temporal Features from Pose Values | 5 |
| 3.2.1 | Distances Between body parts | 6 |
| 3.2.2 | Joint Angles Between body parts | 6 |
| 3.2.3 | Cartesian Pose Values of body parts | 7 |
| 3.2.4 | Constructing Spatio-temporal Feature Matrices | 7 |
| 3.3 | Extending Spatio-temporal Features to Multiple Time-scales | 7 |
| 3.3.1 | Computing Moving Statistics of Gradient Spatio-temporal Features | 8 |
| 3.3.2 | Applying Continuous Wavelet Transformation on Snapshot Spatio-temporal Features | 8 |
| 3.3.3 | Constructing Extended Postural Dynamic Feature Tensors | 10 |
| 3.4 | Computation of Behavioral Representations | 10 |
| 3.4.1 | Flattening of Extended Postural Dynamics Feature Tensors | 10 |
| 3.4.2 | L^1 Normalization of Frames | 10 |
| 3.5 | Summary | 11 |
| 4 | Experiment Outlining | 12 |
| 5 | Behavior Mapping | 13 |
| 5.1 | Computing Behavioral Embeddings | 13 |
| 5.1.1 | Supervised Disparate Embeddings | 13 |
| 5.1.2 | Supervised Joint Embeddings | 13 |
| 5.1.3 | Unsupervised Disparate Embeddings | 14 |
| 5.1.4 | Unsupervised Joint Embedding | 14 |
| 5.1.5 | Semi-supervised Pair Embeddings | 14 |
| 5.2 | Soft Clustering of Behavioral Embeddings | 14 |
| 5.2.1 | Disparate Clustering | 14 |
| 5.2.2 | Joint Clustering | 14 |

| | | |
|-----------|--|-----------|
| 5.2.3 | Crosswise Clustering | 14 |
| 5.3 | Computing Behavioral Correspondences | 15 |
| 5.3.1 | Mapping Clusters to Behavioral Categories | 15 |
| 5.3.2 | Computing Behavioral Scores | 15 |
| 6 | Analyzing Behavioral Repertoire of Asleep Fruit Fly | 16 |
| 7 | Employing Proposed Pipeline for Collected Data | 17 |
| 8 | Results | 18 |
| 9 | basty: A Software Package for Automated <u>B</u>ehavioral <u>A</u>nalysis of Asleep Fruit Fly | 19 |
| 10 | Conclusion | 20 |

List of Figures

| | |
|---|----|
| 1.1 Orientations. | 1 |
| 5.1 Supervised Disparate Embedding. | 13 |

List of Tables

Abstract

A *Basti* (English: *Basty*, Azerbaijani Turkish: *Basdı*, Anatolian Turkish: *Basdırık*) is an evil spirit in Turkic mythology which rides on people's chests while they sleep, bringing on nightmares. *Basti* sits astride a sleeper's chest and becomes heavier until the crushing weight awakens the terrified and breathless dreamer. The victim awakes unable to move under the *Basti*'s weight. It may also include lucid dreams.

Chapter 1

Introduction

1.1 Challenges

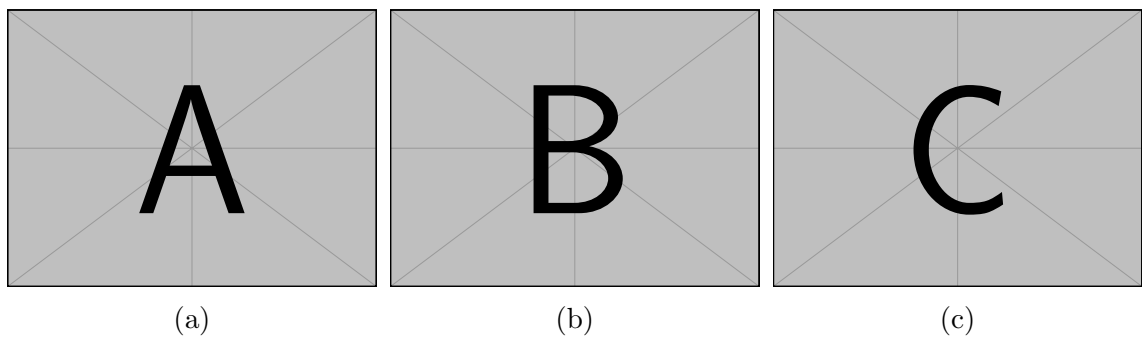


Figure 1.1: Orientations.

1.2 Contributions

Chapter 2

Biological Experiments and Data Collection

Chapter 3

Feature Extraction

For a single experiment data, feature extraction consists of four consecutive steps, where the input in a stage is the output of the previous one. The input of the first step is the raw output signal of the tracking and pose estimation model, in our case, the output of DeepLabCut. The feature extraction steps are as follows:

1. Constructing pose values and preprocessing (filtering and imputation).
2. Computing spatio-temporal features, such as distances between body parts, velocity, angular velocity from body part positions.
3. Extending spatio-temporal features to multiple time-scales using wavelet transformation and sliding window statistics.
4. Computing high-dimensional behavioral representations with normalization.

Matrices $\mathbf{X} \in \mathbb{R}^{T \times N}$ and $\mathbf{Y} \in \mathbb{R}^{T \times N}$ denotes a multivariate time series collected for N tracked body part of the fly on T time stamps by a pose estimation model, respectively for x and y cartesian components of two-dimensional video recordings. This multivariate time series matrices \mathbf{X} and \mathbf{Y} are the raw input data to the first step of the feature extraction. Note that N must be the same among all experiments conducted with different fruit flies, but T might differ. Each column of the $\mathbf{X} = [\mathbf{x}_1, \dots, \mathbf{x}_N]^\top$ and $\mathbf{Y} = [\mathbf{y}_1, \dots, \mathbf{y}_N]^\top$ can be written respectively as follows;

$$\begin{aligned}\mathbf{y}_i &= (y_{i,1}, y_{i,2}, \dots, y_{i,t-1}, y_{i,t}, y_{i,t}, \dots, y_{i,T}), \\ \mathbf{x}_i &= (x_{i,1}, x_{i,2}, \dots, x_{i,t-1}, x_{i,t}, x_{i,t}, \dots, x_{i,T}).\end{aligned}$$

Here i denotes the index of the body part, e.g. leg tip or proboscis.

In addition to \mathbf{X} and \mathbf{Y} , many tracking and pose estimation models report prediction scores for each tracked body part at each time step. $L \in \mathbb{R}^{N \times T}$ denotes the time series of prediction scores, each column of the $L = [l_1, \dots, l_N]^\top$ can be written as follows;

$$\mathbf{l}_i = (l_{i,1}, l_{i,2}, \dots, l_{i,t-1}, l_{i,t}, l_{i,t}, \dots, l_{i,T}).$$

The prediction score drops drastically when the body part is not visible. Thus, L provides valuable information about the occluded body parts. In the Section 3.1.1, how L is incorporated into construction of pose values is described in detail.

3.1 Construction of Pose Values and Preprocessing

The goal of this sub-stage is primarily preprocessing, which involves filtering and imputation certain frames. But in addition to this, there are a couple of optional procedures that can be beneficial for our task of learning stereotypical behaviors. These additional procedures deal with occluded body parts of the fly, alignment of the fly orientations and defining new points of interest.

3.1.1 Dealing with Occluded Body Parts

As mentioned in the Section 1.1, the two-dimensional video recordings introduces a number of important challenges, and one of them is the occluded body part challenge. There are many types of occlusions which can be informally described as follows. One examples is short occlusions resulting from postural changes. Imputation of the time series \mathbf{X} and \mathbf{Y} for these short occlusions is relatively easy since the number of missing data points are few. However, this is not the case for long occlusions which usually occur when the fly is dormant for a long period of time. Especially for the body parts which have left and right counterparts, it is common that the orientation of the fly results in one of the counterparts being occluded in long dormant epochs. We follow multiple approaches to handle different type occlusions; namely imputation and elimination of corresponding data-points. Before describing those approaches we define a criterion for being occluded.

Computing Oriented Pose Values to Handle Body Parts with Left & Right Counterparts

If the fly oriented perpendicular to the camera perspective as in Figure 1.1c, then one of the left and right body parts is often occluded. In other orientations (e.g. Figure 1.1a and Figure 1.1b), both of them or none of them might be occluded as well. However, in the conducted experiments, flies usually choose to stay dormant perpendicular to the camera perspective in long dormant epochs, as mentioned in Chapter 2. In such cases, one can only use one of the left and right counterparts to construct pose values. Therefore, this optional step is included in the behavioral mapping pipeline to reduce pose values of body parts with left and right counterparts to a single value.

We use prediction scores to determine which body part should be used to construct pose value. Let i and j be a pair of body parts which are left and right counterparts of each other, e.g. left haltere and right haltere. Then one can use the \mathbf{l}_i and \mathbf{l}_j to predict if one of them is occluded at a particular time step t . Let $\text{orient}(\mathbf{x}_i, \mathbf{x}_j)$ ($\text{orient}(\mathbf{y}_i, \mathbf{y}_j)$) be a new pose vector which will be computed based on \mathbf{x}_i and \mathbf{x}_j (\mathbf{y}_i and \mathbf{y}_j), e.g. an oriented haltere pose value from left haltere and right haltere. The following conditional produces are proposed to compute oriented pose values from left and right pose values by deciding the orientation of the fly for that counterpart; they can be used separately or together.

- If $l_{i,t} - l_{j,t} \geq \epsilon$ then without loss of generality $\text{orient}(x_{i,t}, x_{j,t}) = x_{i,t}$ and $\text{orient}(y_{i,t}, y_{j,t}) = y_{i,t}$ for a threshold ϵ , typically $\epsilon > 0.5$.

- If $|\{t' \mid l_{i,t'} > l_{j,t'}, t' \in [t-w..t+w]\}| > w$, then without loss of generality $\text{orient}(x_{i,t}, x_{j,t}) = x_{i,t}$ and $\text{orient}(y_{i,t}, y_{j,t}) = y_{i,t}$ for a window size $2w + 1$.
- If $l_{i,t} > l_{j,t}$ and $|t - t^i| < |t - t^j|$ where $t^i = \arg \min_{t'} |t - t'|$, $t^i \in \{t' \mid l_{i,t'} - l_{j,t'} > \epsilon\}$ and $t^j = \arg \min_{t'} |t - t'|$, $t^j \in \{t' \mid l_{j,t'} - l_{i,t'} > \epsilon\}$ for some threshold ϵ then without loss of generality $\text{orient}(x_{i,t}, x_{j,t}) = x_{i,t}$ and $\text{orient}(y_{i,t}, y_{j,t}) = y_{i,t}$.
- If simply $l_{i,t} > l_{j,t}$ (i.e. hard threshold) then without loss of generality $\text{orient}(x_{i,t}, x_{j,t}) = x_{i,t}$ and $\text{orient}(y_{i,t}, y_{j,t}) = y_{i,t}$.

Except applying a hard threshold, all other conditions may leave some of the time points with undecided orientations. If the number of such time points is acceptable, then applying hard threshold for those time points is convenient and handy.

After applying above procedures for one right and left counterpart pair i, j , we can define

$$\begin{aligned}\mathbf{X}^* &= \left([(\mathbf{x}_p)_{p \notin \cup \mathcal{O}}] \mid [(\text{orient}(\mathbf{x}_i, \mathbf{x}_j))_{\{i,j\} \in \mathcal{O}}] \right)^\top, \\ \mathbf{Y}^* &= \left([(\mathbf{y}_p)_{p \notin \cup \mathcal{O}}] \mid [(\text{orient}(\mathbf{y}_i, \mathbf{y}_j))_{\{i,j\} \in \cup \mathcal{O}}] \right)^\top.\end{aligned}$$

$$\begin{aligned}\mathbf{X}^* &= \left((x_{p,t})_{t \in \{1, \dots, T\}, p \notin \cup \mathcal{O}} \mid [(\text{orient}(\mathbf{x}_i, \mathbf{x}_j))_{\{i,j\} \in \mathcal{O}}] \right)^\top, \\ \mathbf{Y}^* &= \left((y_{p,t})_{t \in \{1, \dots, T\}, p \notin \cup \mathcal{O}} \mid [(\text{orient}(\mathbf{y}_i, \mathbf{y}_j))_{\{i,j\} \in \mathcal{O}}] \right)^\top.\end{aligned}$$

where \mathcal{O} is the set of index pairs of right and left counterparts and $\cup \mathcal{O}$ is the union of all such indexes. Applying this procedure for each right and left counterparts results in computing \mathbf{X}^* and \mathbf{Y}^* . This oriented version of original data matrices can be used instead of \mathbf{X} and \mathbf{Y} in the rest of the pipeline, if desired.

Detecting Occlusions Using Prediction Scores and Preternatural Tracking Predictions

3.1.2 Aligning Flies with Different Orientations

3.1.3 Preprocessing: Filtering and Imputation

3.2 Computation of Spatio-temporal Features from Pose Values

Constructing pose values enables us to go one step further towards learning stereotypical behaviors. Tracking of relevant body parts and constructing pose values is an essential step for quantifying behavior. However, a set of coordinate values is sufficient to describe and represent complex spatio-temporal dynamics of animal behavior. There are thousands of unique postures and behaviors are not exhibited by some static set of postures. Instead, they are defined by expressive and meaningful

spatio-temporal features such as distances, velocities, angles and angular velocities. Therefor, one need to compute such features from the coordinate values of body parts in two dimensional space.

Second stage of the feature extraction is computation of spatio-temporal features from pose values. Two type of features are computed in this stage.

1. **Snapshot features:** Spatio-temporal feature values computed at a snapshot of time.

- distances,
- angles,
- cartesian pose values (i.e. per body part features).

2. **Gradient features:** Spatio-temporal feature values computed based how snap features change over time.

- change of distances,
- change of angles (i.e. angular velocities),
- change of cartesian pose values (i.e. body part velocities).

The gradient of snapshot features computed using second order accurate central differences in the interior points. The returned gradient features has the same shape as the snapshot features.

3.2.1 Distances Between body parts

Given body part pair (i, j) , distances between them at a time step t is computed as:

$$d_t^{i,j} = \sqrt{(x_{i,t} - x_{j,t})^2 + (y_{i,t} - y_{j,t})^2}. \quad (3.1)$$

The corresponding gradient feature, which is the change of distance between body part i and j is computed as follows using the second order gradient approximation:

$$\dot{d}_t^{i,j} = \begin{cases} \frac{|d_{t+1}^{i,j} - d_t^{i,j}|}{\Delta t} & \text{if } t=0 \text{ or } t=T, \\ \frac{|d_{t+1}^{i,j} - d_{t-1}^{i,j}|}{2\Delta t} & \text{otherwise,} \end{cases} \quad (3.2)$$

where Δt is the sampling period, which is equal to $1/\text{FPS}$ seconds.

3.2.2 Joint Angles Between body parts

Given a triplet of body parts (i, j, k) , angle between i and k around j is computed using the 2-argument arctangent function as below.

$$w_t^{i,j,k} = \text{atan2} \left(\det \begin{bmatrix} x_{i,t} - x_{j,t}, x_{k,t} - x_{j,t} \\ y_{i,t} - y_{j,t}, y_{k,t} - y_{j,t} \end{bmatrix}, \begin{bmatrix} x_{i,t} - x_{j,t} \\ y_{i,t} - y_{j,t} \end{bmatrix} \cdot \begin{bmatrix} x_{k,t} - x_{j,t} \\ y_{k,t} - y_{j,t} \end{bmatrix} \right) + \pi \quad (3.3)$$

Then similar to distance gradient feature, angular velocity is approximated by:

$$\dot{w}_t^{i,j,k} = \begin{cases} \frac{|w_{t+1}^{i,j,k} - w_t^{i,j,k}|}{\Delta t} & \text{if } t=0 \text{ or } t=T, \\ \frac{|w_{t+1}^{i,j,k} - w_{t-1}^{i,j,k}|}{2\Delta t} & \text{otherwise.} \end{cases} \quad (3.4)$$

3.2.3 Cartesian Pose Values of body parts

Cartesian pose values of a body part i is straightforwardly given by the x and y coordinate values:

$$x_t^i = x_{i,t}, \quad (3.5)$$

$$y_t^i = y_{i,t}. \quad (3.6)$$

Note that for a single body part two feature values is generated.

Corresponding gradient features, namely body part velocities along each cartesian component is computed as follows:

$$\dot{x}_t^i = \begin{cases} \frac{x_{t+1}^i - x_t^i}{\Delta t} & \text{if } t=0 \text{ or } t=T, \\ \frac{x_{t+1}^i - x_{t-1}^i}{2\Delta t} & \text{otherwise,} \end{cases} \quad (3.7)$$

$$\dot{y}_t^i = \begin{cases} \frac{y_{t+1}^i - y_t^i}{\Delta t} & \text{if } t=0 \text{ or } t=T, \\ \frac{y_{t+1}^i - y_{t-1}^i}{2\Delta t} & \text{otherwise.} \end{cases} \quad (3.8)$$

3.2.4 Constructing Spatio-temporal Feature Matrices

Let \mathcal{C} , \mathcal{D} , and \mathcal{A} denote set of body parts, body part pairs, body part triplets which defines snapshot features; respectively cartesian pose values, distances and angles. Similarly, let \mathcal{C}' , \mathcal{D}' , and \mathcal{A}' denote sets which define sets respective gradient features. Then snapshot feature matrix S constructed as follows;

$$\mathbf{S} = (x_t^i)_{1 \leq t \leq T, i \in \mathcal{C}} \mid (y_t^i)_{1 \leq t \leq T, i \in \mathcal{C}} \mid (d_t^{i,j})_{1 \leq t \leq T, \{i,j\} \in \mathcal{D}} \mid (w_t^{i,j,k})_{1 \leq t \leq T, \{i,j,k\} \in \mathcal{A}}. \quad (3.9)$$

Similarly for gradient features, feature matrix is constructed by concatenating change of distances, change of angles and body part velocities;

$$\mathbf{V} = (\dot{x}_t^i)_{1 \leq t \leq T, i \in \mathcal{C}'} \mid (\dot{y}_t^i)_{1 \leq t \leq T, i \in \mathcal{C}'} \mid (d_t^{i,j})_{1 \leq t \leq T, \{i,j\} \in \mathcal{D}'} \mid (w_t^{i,j,k})_{1 \leq t \leq T, \{i,j,k\} \in \mathcal{A}'} . \quad (3.10)$$

The resulting two feature matrices are $\mathbf{S} \in \mathbb{R}^{T \times (|\mathcal{C}| \cdot |\mathcal{D}| \cdot |\mathcal{A}|)}$ and $\mathbf{V} \in \mathbb{R}^{T \times (|\mathcal{C}'| \cdot |\mathcal{D}'| \cdot |\mathcal{A}'|)}$. Let N_s denote the number of snapshot features, being equal to $|\mathcal{C}| \cdot |\mathcal{D}| \cdot |\mathcal{A}|$ and let N_v denote number of gradient features which is equal to $|\mathcal{C}'| \cdot |\mathcal{D}'| \cdot |\mathcal{A}'|$.

3.3 Extending Spatio-temporal Features to Multiple Time-scales

Instantaneous values of spatio-temporal features do not provide sufficient description of behavior. Understanding of output of a complex biological system, in our case behavior, can only be achieved by studying multiple time-scale together. Previous studies attempt to search behavioral motifs, e.g. repeated sub-sequences of actions with finite length, within the behavioral time series. However, as Berman et al. [2014] states, this paradigm usually requires problems of temporal alignment and relative phasing between different scales. Alternatively, extending spatio-temporal features to capture postural dynamics at different time-scale eliminate requirements of temporal alignment and motif based analysis. In order to extend the spatio-temporal

features, we applied wavelet transformation (similar to Berman et al. [2014]) and computed moving statistics at different time scales (similar to Kabra et al. [2013]), respectively for snapshot feature set (\mathbf{S}) and gradient feature set (\mathbf{V}).

3.3.1 Computing Moving Statistics of Gradient Spatio-temporal Features

Gradient features only reflects the instantaneous values of velocities with respect to the sampling rate. In order to capture how these values change within a given interval, the moving statistics, e.g. mean and standard deviation, of gradient features are computed with a sliding window approach. Let τ be the window size parameter, i.e. the considered time scale, then moving mean of the corresponding gradient feature \mathbf{v}_i is given by function μ_τ as:

$$\mu_\tau(v_{i,t}) = \frac{1}{\min\{t + \tau, T\} - \max\{t - \tau, 1\} + 1} \sum_{t'=\max\{t-\tau,1\}}^{\min\{t+\tau,T\}} v_{i,t'}. \quad (3.11)$$

Similarly the moving standard deviation of a gradient feature $v_{i,t}$ by σ_τ as follows:

$$\sigma_\tau(v_{i,t}) = \sqrt{\frac{1}{\min\{t + \tau, T\} - \max\{t - \tau, 1\} + 1} \sum_{t'=\max\{t-\tau,1\}}^{\min\{t+\tau,T\}} (\mu_\tau(v_{i,t}) - v_{i,t'})^2}. \quad (3.12)$$

This feature generation approach is used to learn animal behavior by Kabra et al. [2013], and Marshall et al. [2021] is also included such features into the analysis.

3.3.2 Applying Continuous Wavelet Transformation on Snapshot Spatio-temporal Features

The wavelet domain is a useful representation of postural dynamics due to the following reasons given by Berman et al. [2014], and proposed spectrogram generation is used by others as well [Marshall et al., 2021, Todd et al., 2017].

1. It describes dynamics over multiple time scales simultaneously by possessing a multi-resolution time-frequency trade-off.
2. It eliminates the requirement of precise temporal alignment for capturing periodic behaviors by taking amplitudes of the continuous wavelet transform for each snapshot feature.

Given a function $s(t)$, continuous wavelet transformation at a frequency $f > 0$ is expressed by following integral;

$$W_{f,t'}[s(t)] = \frac{1}{\sqrt{a(f)}} \int_{-\infty}^{\infty} s(t') \Psi^* \left(\frac{t' - t}{a(f)} \right) dt', \quad (3.13)$$

where Ψ is the wavelet function and a is a function for converting frequencies to wavelet scale factor. The Morlet wavelet is suitable for describing postural dynamics

which is closely related to human perception, both hearing and vision [Daugman, 1985]. The corresponding wavelet function is given by

$$\Psi(t) = \exp\left\{\frac{t^2}{2}\right\} \cos(w_0 t), \quad (3.14)$$

where w_0 is a non-dimensional. The corresponding function a for Morlet wavelet is as follows;

$$s(f) = \frac{w_0 + \sqrt{2 + w_0^2}}{4\pi f}, \quad (3.15)$$

For the discrete sequence of snapshot feature \mathbf{s}_i with sampling period Δt , $W_{f,t}[s(t)]$ translates into;

$$W_f(\mathbf{s}_i, t) = \frac{1}{\sqrt{a(f)}} \sum_{t'=1}^T \Delta t s_{i,t'} \Psi^* \left(\frac{t' - t}{af} \right), \quad (3.16)$$

where $t \in \mathbb{Z}$ [Torrence and Compo, 1998].

Normalization of Wavelet Power Spectrum

In order to ensure that wavelet transforms (Equation 3.16) at each frequency f are directly comparable to each other and to the other transformed time series, the transformation W_f has to be normalized at each frequency f to have unit energy. This normalization for Morlet wavelet at frequency f is given by

$$C(f) = \frac{\pi^{-\frac{1}{4}}}{\sqrt{2a(f)}} \exp\left\{ \frac{1}{4} \left(w_0 - \sqrt{w_0^2 + 2} \right)^2 \right\}. \quad (3.17)$$

So resulting normalized transformation which is also considered to spectrogram generation in Berman et al. [2014] is given by

$$W_f^0(\mathbf{s}_i, t) = \frac{1}{C(f)} |W_f(\mathbf{s}_i, t)|. \quad (3.18)$$

In addition to above conventionally used normalization, we alternatively adopted normalization proposed by Liu et al. [2007]. According to this alternative adjustment, wavelet power spectrum should be the transform coefficient squared divided by the scale it associates.

$$W_f^0(\mathbf{s}_i, t) = \frac{W_f(\mathbf{s}_i, t)^2}{a(f)} \quad (3.19)$$

We observed substantial improvements using this power spectrum (see Section 7).

Determining Spectrum Frequencies

We investigate two different approaches for computing set of frequencies and, we include both of them in the behavior mapping pipeline. One set is dyadically spaced frequencies between f_{\min} and f_{\max} via;

$$f_i = f_{\max} 2^{-\frac{i-1}{N_f-1} \log \frac{f_{\max}}{f_{\min}}}, \quad (3.20)$$

where $f_{\max} = \text{FPS}/2$ Hz is the Nyquist frequency.

The other alternative set of frequencies is linearly spaced between f_{\min} and f_{\max} by

$$f_i = f_{\min} + \frac{f_{\max} - f_{\min}}{N_f - 1} i, \quad (3.21)$$

for $i = 1, 2, \dots, N_f$, and their corresponding wavelet scales are computed via $a(f_i)$.

3.3.3 Constructing Extended Postural Dynamic Feature Tensors

Let $\mathcal{T}_s = \{1/f_{\min}, \dots, 1/f_{\max}\}$ and $\mathcal{T}_v = \{\tau_{\min}, \dots, \tau_{\max}\}$ denote the time scale sets respectively for wavelet transformed snapshot features and moving statistics of gradient features. Then corresponding feature tensors are given as follows:

$$\mathbf{W} = [W_{1/\tau}^0(\mathbf{s}_i, t)]_{1 \leq i \leq N_s, 1 \leq t \leq T, \tau \in \mathcal{T}_s}, \quad (3.22)$$

$$\mathbf{M}_\mu = [\mu_\tau(v_{i,t})]_{1 \leq i \leq N_v, 1 \leq t \leq T, \tau \in \mathcal{T}_v}, \quad (3.23)$$

$$\mathbf{M}_\sigma = [\sigma_\tau(v_{i,t})]_{1 \leq i \leq N_v, 1 \leq t \leq T, \tau \in \mathcal{T}_v}, \quad (3.24)$$

where $\mathbf{S} \in \mathbb{R}^{T \times N_s}$ and $\mathbf{V} \in \mathbb{R}^{T \times N_v}$.

The resulting extended feature tensors of postural dynamic representations are $\mathbf{W} \in \mathbb{R}^{T \times |\mathcal{T}_s| \times N_s}$, $\mathbf{M}_\mu \in \mathbb{R}^{T \times |\mathcal{T}_v| \times N_v}$ and $\mathbf{M}_\sigma \in \mathbb{R}^{T \times |\mathcal{T}_v| \times N_v}$.

3.4 Computation of Behavioral Representations

After applying wavelet transformation or computing moving statistics to extend extracted spatio-temporal features to postural dynamics features, couple of additional operations are required to generate desired embeddings.

3.4.1 Flattening of Extended Postural Dynamics Feature Tensors

As mentioned in Section 3.3, feature tensors are $\mathbf{W} \in \mathbb{R}^{T \times |\mathcal{T}_s| \times N_s}$, $\mathbf{M}_\mu \in \mathbb{R}^{T \times |\mathcal{T}_v| \times N_v}$, and $\mathbf{M}_\sigma \in \mathbb{R}^{T \times |\mathcal{T}_v| \times N_v}$. In order to apply manifold learning based dimensionality reduction algorithms or traditional machine learning algorithms such as decision trees, one need to flatten last two dimensions of these postural dynamics feature tensors. As a result, feature matrices are $\mathbf{W}^* \in \mathbb{R}^{T \times (N_s|\mathcal{T}_s|)}$, $\mathbf{M}_\mu^* \in \mathbb{R}^{T \times (N_v|\mathcal{T}_v|)}$ and $\mathbf{M}_\sigma^* \in \mathbb{R}^{T \times (N_v|\mathcal{T}_v|)}$ are obtained.

3.4.2 L^1 Normalization of Frames

Wavelet power spectrum and gradient feature values are heavily dependent on the orientation of the flies and on the unique fly characteristics. In order to have a homogeneous feature space among flies and along the time, at each time step t , L^1 normalization is applied as follows;

$$\mathbf{W}' = \left(\frac{w_{t,i}^*}{\sum_{j=0}^{N_s|\mathcal{T}_s|} w_{t,j}^*} \right)_{1 \leq t \leq T, 1 \leq i \leq (N_s|\mathcal{T}_s|)}. \quad (3.25)$$

Similarly, L^1 normalized versions of \mathbf{M}_μ^* and \mathbf{M}_σ^* , namely \mathbf{M}'_μ and $\mathbf{M}'\sigma$ are obtained.

Here \mathbf{W}' , \mathbf{M}'_μ and $\mathbf{M}'\sigma$ are the final multivariate time series of normalized high dimensional behavioral representation of a fly experiment. Behavioral representation matrix \mathbf{W}' will be used to compute behavioral embeddings.

3.5 Summary

Chapter 4

Experiment Outlining

Chapter 5

Behavior Mapping

5.1 Computing Behavioral Embeddings

McInnes et al. [2020] McInnes et al. [2017] Campello et al. [2013]

5.1.1 Supervised Disparate Embeddings

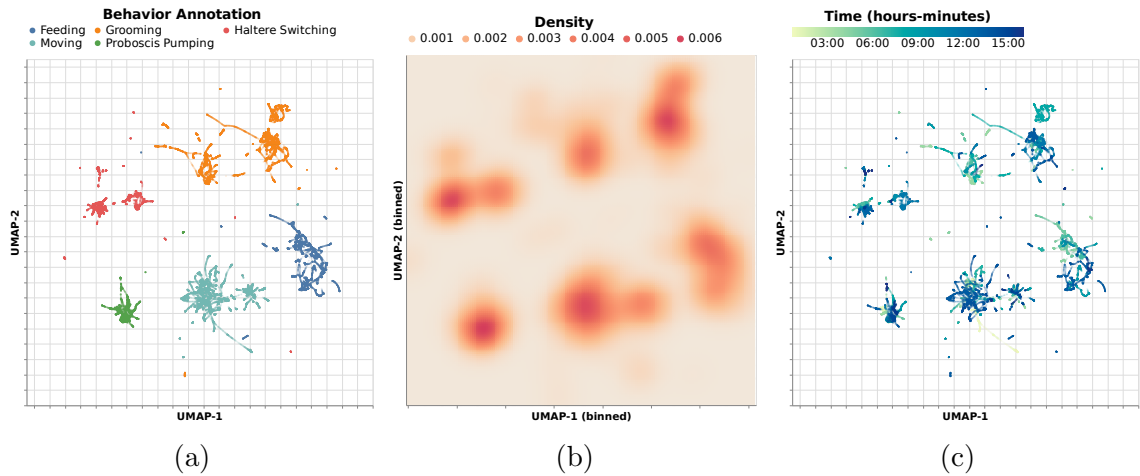


Figure 5.1: Supervised Disparate Embedding.

[NOTE: We compute Supervised-UMAP embeddings separately for each experiment. Computing supervised embeddings is only possible for annotated experiments. This is useful for exploring behavioral sub-categories. For instance, one annotation category, e.g. "grooming", can be consisted of two different clusters in the behavioral embedding space. We can further investigate how high-level behavioral annotations contain different but similar behaviors.]

5.1.2 Supervised Joint Embeddings

[NOTE: We compute Supervised-UMAP embeddings of all annotated experiments together. There is no specific benefit or use case (except visualization purposes) for computing this. The resulting embedding usually is not homogeneous in terms of fly experiments. Different flies do not mix well in the behavioral space.]

5.1.3 Unsupervised Disparate Embeddings

[NOTE: For each experiment, we compute a usual unsupervised embedding separately.]

5.1.4 Unsupervised Joint Embedding

[NOTE: We compute a single behavioral embedding using all experiments. The problem with this approach is that embedding space is too crowded and thus we can not find meaningful and homogeneous clusters right away. This embedding might be useful for visualization purposes.]

5.1.5 Semi-supervised Pair Embeddings

[NOTE: This is the novel and most useful embedding approach that we finally utilize to label unannotated experiments using annotated ones. We compute an embedding for each annotated and unannotated pair. For example, if there are N_A annotated experiments and N_U unannotated experiments we compute $N_A \cdot N_U$ embeddings in total. There are number of advantageous of this approach. Especially when, an behavioral repertoire of an annotated an unannotated are similar, resulting embedding is easy to interpret and use for clustering etc.]

5.2 Soft Clustering of Behavioral Embeddings

[NOTE: We always use soft clustering feature of HDBSCAN, since it is very beneficial to have a composite assignment for a data-point. For example, 0.7 grooming, 0.3 proboscis pumping may indicate that those two behaviors are simultaneously exhibited or a combination of both is exhibited etc. We can always take arg max if a categorical label is needed.]

5.2.1 Disparate Clustering

[NOTE: If embedding is a disparate embedding, then we directly cluster each of them separately. If a joint embedding or pair embedding will be clustered, then experiments need to be extracted from the embedding space first and then they need to be clustered separately.]

5.2.2 Joint Clustering

[NOTE: This is only applicable to joint and pair embeddings. We cluster all experiments in the behavioral embedding together.]

5.2.3 Crosswise Clustering

[NOTE: This is again only applicable to joint and pair embeddings. For joint embeddings, we exclude a sub-group of experiments. For pair embeddings, we exclude one of the pair experiments. Then rest of the embedding is clustered and clusters are formed. Finally for each excluded embedding, soft cluster memberships vectors are computed based on the formed clusters.]

5.3 Computing Behavioral Correspondences

5.3.1 Mapping Clusters to Behavioral Categories

[NOTE: If a clustering contains annotated experiments, we map that clusters in that clustering to a behavioral composition as follows (*subject to change, there are couple of alternatives*)

$$m_\alpha = \frac{\text{number of frames with annotation } \alpha \text{ in the cluster}}{\text{total number of frames with annotation } \alpha}. \quad (5.1)$$

So for each cluster, we end up with a vector $\mathbf{m} = (m_\alpha)$, represent it behavioral composition.]

5.3.2 Computing Behavioral Scores

[NOTE: Behavioral score of unannotated experiment will be computed using clustering membership score and behavioral composition mapping of those clusters. For example, using semi-supervised pair embeddings and crosswise clustering; one can compute behavioral scores for a frame as follows;

$$y_\alpha = \sum_{c=0}^C m_\alpha^c \quad (5.2)$$

where C is the number of clusters, \mathbf{m}^c is the behavioral composition of cluster c . As a result, for each frame we end up with a behavioral score vector $\mathbf{y} = (y_\alpha)$.]

Chapter 6

Analyzing Behavioral Repertoire of Asleep Fruit Fly

Chapter 7

Employing Proposed Pipeline for Collected Data

Chapter 8

Results

Chapter 9

basty: A Software Package for
Automated Behavioral Analysis of
Asleep Fruit Fly

Chapter 10

Conclusion

Bibliography

- Gordon J. Berman, Daniel M. Choi, William Bialek, and Joshua W. Shaevitz. Mapping the stereotyped behaviour of freely moving fruit flies. *Journal of The Royal Society Interface*, 11(99):20140672, October 2014. doi: 10.1098/rsif.2014.0672. URL <https://royalsocietypublishing.org/doi/full/10.1098/rsif.2014.0672>. Publisher: Royal Society.
- Mayank Kabra, Alice A. Robie, Marta Rivera-Alba, Steven Branson, and Kristin Branson. JAABA: interactive machine learning for automatic annotation of animal behavior. *Nature Methods*, 10(1):64–67, January 2013. ISSN 1548-7105. doi: 10.1038/nmeth.2281. URL <https://www.nature.com/articles/nmeth.2281>. Number: 1 Publisher: Nature Publishing Group.
- Jesse D. Marshall, Diego E. Aldarondo, Timothy W. Dunn, William L. Wang, Gordon J. Berman, and Bence P. Ölveczky. Continuous Whole-Body 3D Kinematic Recordings across the Rodent Behavioral Repertoire - SI. *Neuron*, 109(3):420–437.e8, February 2021. ISSN 08966273. doi: 10.1016/j.neuron.2020.11.016. URL <https://linkinghub.elsevier.com/retrieve/pii/S0896627320308941>.
- Jeremy G. Todd, Jamey S. Kain, and Benjamin L. de Bivort. Systematic exploration of unsupervised methods for mapping behavior. *Physical Biology*, 14(1):015002, February 2017. ISSN 1478-3975. doi: 10.1088/1478-3975/14/1/015002. URL <https://doi.org/10.1088/1478-3975/14/1/015002>. Publisher: IOP Publishing.
- John G. Daugman. Uncertainty relation for resolution in space, spatial frequency, and orientation optimized by two-dimensional visual cortical filters. *JOSA A*, 2(7):1160–1169, July 1985. ISSN 1520-8532. doi: 10.1364/JOSAA.2.001160. URL <https://opg.optica.org/josaa/abstract.cfm?uri=josaa-2-7-1160>. Publisher: Optica Publishing Group.
- Christopher Torrence and Gilbert P. Compo. A Practical Guide to Wavelet Analysis. *Bulletin of the American Meteorological Society*, 79(1):61–78, January 1998. ISSN 0003-0007, 1520-0477. doi: 10.1175/1520-0477(1998)079<0061:APGTWA>2.0.CO;2. URL [http://journals.ametsoc.org/doi/10.1175/1520-0477\(1998\)079<0061:APGTWA>2.0.CO;2](http://journals.ametsoc.org/doi/10.1175/1520-0477(1998)079<0061:APGTWA>2.0.CO;2).
- Yonggang Liu, X. San Liang, and Robert H. Weisberg. Rectification of the Bias in the Wavelet Power Spectrum. *Journal of Atmospheric and Oceanic Technology*, 24(12):2093–2102, December 2007. ISSN 1520-0426, 0739-0572. doi: 10.1175/2007JTECHO511.1. URL <http://journals.ametsoc.org/doi/10.1175/2007JTECHO511.1>.

Leland McInnes, John Healy, and James Melville. UMAP: Uniform Manifold Approximation and Projection for Dimension Reduction. *arXiv:1802.03426 [cs, stat]*, September 2020. URL <http://arxiv.org/abs/1802.03426>. arXiv: 1802.03426.

Leland McInnes, John Healy, and Steve Astels. hdbscan: Hierarchical density based clustering. *Journal of Open Source Software*, 2(11):205, March 2017. ISSN 2475-9066. doi: 10.21105/joss.00205. URL <https://joss.theoj.org/papers/10.21105/joss.00205>.

Ricardo J. G. B. Campello, Davoud Moulavi, and Joerg Sander. Density-Based Clustering Based on Hierarchical Density Estimates. In Jian Pei, Vincent S. Tseng, Longbing Cao, Hiroshi Motoda, and Guandong Xu, editors, *Advances in Knowledge Discovery and Data Mining*, Lecture Notes in Computer Science, pages 160–172, Berlin, Heidelberg, 2013. Springer. ISBN 978-3-642-37456-2. doi: 10.1007/978-3-642-37456-2_14.